

## Research



**Cite this article:** Tolentino L, Yigeremu M, Teklu S, Attia S, Weiler M, Frank N, Dixon JB, Gleason Jr RL. 2019 Three-dimensional camera anthropometry to assess risk of cephalopelvic disproportion-related obstructed labour in Ethiopia. *Interface Focus* **9**: 20190036. <http://dx.doi.org/10.1098/rsfs.2019.0036>

Accepted: 29 May 2019

One contribution of 15 to a theme issue 'Bioengineering in women's health, volume 2: pregnancy—from implantation to parturition'.

### Subject Areas:

bioengineering

### Keywords:

obstructed labour, pregnancy risk, low-cost diagnostic, developing world, anthropometry

### Author for correspondence:

Rudolph L. Gleason Jr  
e-mail: [rudy.gleason@me.gatech.edu](mailto:rudy.gleason@me.gatech.edu)

Electronic supplementary material is available online at <https://dx.doi.org/10.6084/m9.figshare.c.4533317>.

# Three-dimensional camera anthropometry to assess risk of cephalopelvic disproportion-related obstructed labour in Ethiopia

Lorenzo Tolentino<sup>1</sup>, Mahlet Yigeremu<sup>2</sup>, Sisay Teklu<sup>2</sup>, Shehab Attia<sup>3</sup>, Michael Weiler<sup>4</sup>, Nate Frank<sup>4</sup>, J. Brandon Dixon<sup>4,5</sup> and Rudolph L. Gleason Jr<sup>1,3,5</sup>

<sup>1</sup>Because of Kennedy, Inc., Acworth, GA, USA

<sup>2</sup>Department of Obstetrics and Gynecology, Addis Ababa University, Addis Ababa, Ethiopia

<sup>3</sup>The Wallace H. Coulter Department of Biomedical Engineering, Atlanta, GA, USA

<sup>4</sup>LymphaTech, Inc., Atlanta, GA, USA

<sup>5</sup>The George W. Woodruff School of Mechanical Engineering, Atlanta, GA, USA

RLG, 0000-0002-6357-4955

Cephalopelvic disproportion (CPD)-related obstructed labour requires delivery via Caesarean section (C/S); however, in low-resource settings around the world, facilities with C/S capabilities are often far away. This paper reports three low-cost tools to assess the risk of CPD, well before labour, to provide adequate time for referral and planning for delivery. We performed tape measurement- and three-dimensional (3D) camera-based anthropometry, using two 3D cameras (Kinect and Structure) on primigravida, gestational age  $\geq 36$  weeks, from Addis Ababa, Ethiopia. Novel risk scores were developed and tested to identify models with the highest predicted area under the receiver-operator characteristic curve (AUC), detection rate (true positive rate at a 5% false-positive rate, FPR) and triage rate (true negative rate at a 0% false-negative rate). For tape measure, Kinect and Structure, the detection rates were 53%, 61% and 64% (at 5% FPR), the triage rates were 30%, 56% and 63%, and the AUCs were 0.871, 0.908 and 0.918, respectively. Detection rates were 77%, 80% and 84% at the maximum  $J$ -statistic, which corresponded to FPRs of 10%, 15% and 11%, respectively, for tape measure, Kinect and Structure. Thus, tape measurement anthropometry was a very good predictor and Kinect and Structure anthropometry were excellent predictors of CPD risk.

## 1. Introduction

Ethiopia had the fourth highest number of maternal deaths worldwide in 2015 [1]. One out of every 64 Ethiopian women die due to complications with pregnancy and 17% of deaths of 15- to 49-year-old Ethiopian women are due to maternal causes [1,2]. The maternal mortality ratios (MMRs), in Ethiopia and across the world, have significantly improved over the past 25 years; however, in 2015, the MMR of 353 deaths per 100 000 live births in Ethiopia is five times higher than Sustainable Development Goal 3.1; namely, the goal to reduce the global MMR to less than 70 per 100 000 live births by 2030. The percentage of deliveries attended by skilled health professionals in Ethiopia is far below the sub-Saharan Africa and worldwide percentages. In 2005, only 6% of deliveries were attended by a skilled health provider; although this percentage increased in the 2016 survey to 28%, Ethiopia remains far below the sub-Saharan Africa and worldwide percentages of 52% and 71%, respectively, and maintains a large gap between rural and urban areas. The cultural aspect of at-home deliveries likely plays an important role in Ethiopia's subpar percentage of attended

deliveries. These numbers parallel the low uptake in antenatal care (ANC). In 2015, only 62% of pregnant Ethiopian women sought at least one ANC visit and less than 32% sought four or more ANC visits, compared to 49% of women in sub-Saharan Africa who sought four or more ANC visits [1,2].

Cephalopelvic disproportion (CPD) is an inadequate size of the maternal pelvis, compared to the fetal head, which prevents the fetus from passing through the pelvic cavity during delivery, causing obstructed labour [3]. Obstructed labour accounts for 3–8% of the maternal deaths worldwide and 11% of maternal deaths in Ethiopia [4,5]; however, in some regions of Ethiopia, up to 22% of maternal deaths may be attributed to obstructed labour [6–8]. CPD prevalence increases in regions where girls are small in stature, grow up malnourished, marry at a young age and become pregnant before the pelvis is fully grown [9,10], all of which are common in Ethiopia. For example, in a cross-sectional study of obstetric fistula patients in Ethiopia, the mean ages at the first marriage and at the delivery that caused the fistula were 14.7 and 17.8 years, respectively [11]. Indeed, 13% of the girls surveyed in the study in 2016 between 15 and 19 years of age had begun childbearing, including 1.6% of 15-year-olds, 4.4% of 16-year-olds and 13% of 17-year-olds [2].

CPD-related obstructed labour requires delivery via Caesarean section (C/S). In rural Ethiopia and many low-resource settings around the world, it may require hours or days of travel for mothers to reach facilities with the infrastructure and expertise to perform a C/S. After the onset of labour, it is too late for the mother to travel to these facilities for a C/S and the consequence of CPD-related obstructive labour (in the absence of C/S) is often maternal and/or perinatal mortality or long-term morbidity. Maternal mortality occurs via haemorrhage, puerperal sepsis or rupture of the uterus; perinatal conditions include fetal asphyxia, fetal distress, intracranial haemorrhage and hypoxic ischaemic encephalopathy. Long-term maternal morbidity from obstructed labour includes trauma to the bladder that can lead to stress incontinence and obstetric fistulas. An obstetric fistula is a hole that forms in the vaginal wall communicating into the bladder (vesico-vaginal fistula) or the rectum (recto-vaginal fistula), or both [9,12], resulting in urine and/or bowel contents passing uncontrollably through the vagina. In Ethiopia, 1 out of every 250 women report having an obstetric fistula from obstructed labour [2]. Women who develop fistulas are often socially rejected. In one Ethiopian study, more than 50% of the women were rejected and left by their husbands after the fistulae developed [13]. Thus, the consequences of undiagnosed CPD-related obstructed labour go far beyond maternal and perinatal mortality, affecting a significant fraction of the population.

Over the last century, much effort has been dedicated to developing methods to accurately assess the risk of CPD. Clinical pelvimetry requires highly skilled personnel, is subjective and shows low predictive capability. MRI- and CT-pelvimetry are cost prohibitive in low-resource settings and X-ray-pelvimetry poses an unwanted radiation exposure to the fetus. Published anthropometry-based CPD risk scores show only fair predictability. Recently, we demonstrated the feasibility of using a low-cost KinectV2 three-dimensional (3D) camera (Microsoft, Inc.) to generate 3D models of pregnant women, from which anthropometric features are automatically extracted via novel image processing algorithms and used to

calculate a novel CPD risk score to identify at-risk mothers [14]. Our novel 3D camera-based CPD risk score performed on-par with our novel MRI-based CPD risk score and outperformed published CPD risk scores based on radiological pelvimetry, clinical pelvimetry and anthropometry. Further, our novel tape measure-based anthropometry risk score showed very good predictive capabilities, albeit not as predictive as the 3D camera-based score.

The goal of this paper is to develop and test three novel tools to assess the risk of CPD-related obstructed labour in primigravida; namely, (i) a Kinect V2 sensor (Microsoft, Inc., developed for the Xbox gaming system), combined with a laptop computer, (ii) a Structure 3D camera (Occipital, Inc.), combined with an iOS or Android-based smartphone, and (iii) a tape measure-based anthropometry tool (figure 1). The Kinect and Structure 3D cameras generate digital 3D geometric models of pregnant women, from which anthropometric measurements are automatically extracted via novel image processing algorithms and are used to calculate novel CPD risk scores to identify at-risk mothers. We extend our previous work in several important ways. First, we employ a new 3D camera (Structure), which is smartphone-compatible, offers higher resolution images, and easier image-to-3D model acquisition compared to the Kinect. Second, we studied a larger sample set, consisting of only first-time mothers who tried labour. First-time mothers represent the most important group to assess risk, since they lack previous obstetric history and are at the highest risk for CPD-related obstructed labour. Our central hypothesis is that risk scores based on measurements taken with 3D camera and tape measurements from Ethiopian primigravidae between 36 and 42 weeks of gestation can predict the risk of CPD-related obstructed labour, with a detection rate above 60% at a 5% false-positive rate, a triage rate above 60% at a 0% false-negative rate and an area under the receiver operator curve above 0.90.

## 2. Material and methods

### 2.1. Participant enrolment and data collection procedure

This study was approved by the Institutional Review Board at Addis Ababa University, College of Health Sciences (Protocol number: 054/15/gyn, approved on 3 January 2017). Primigravida, 18–40 years of age, at gestational age 36 + 0 weeks or above with vertex presentation and singleton pregnancy were recruited from Tikur Anbessa Specialized Referral Hospital, Girar Health Center and Worreda 08 Health Center in Addis Ababa, Ethiopia. We recruited 685 subjects to participate and combined these data with the data from 148 primigravida from Gleason *et al.* [14]; in [14], anthropometric measurements and Kinect 3D images were collected, but Structure 3D images were not collected.

Participants entered the exam room and a nurse fully informed the participant of the study and obtained written informed consent. The nurse recorded the participant information, including hospital card number, age and gestational age. The nurse confirmed that the subject satisfies the inclusion/exclusion criteria (i.e. primigravida, singleton pregnancy, vertex presentation, plan for trial of labour, plan to deliver in a health facility). *Height* and *weight* were measured with a stadiometer and calibrated scale. Tape measurements of *shoulder height*, *waist height*, *hip height*, *head circumference*, *shoulder*

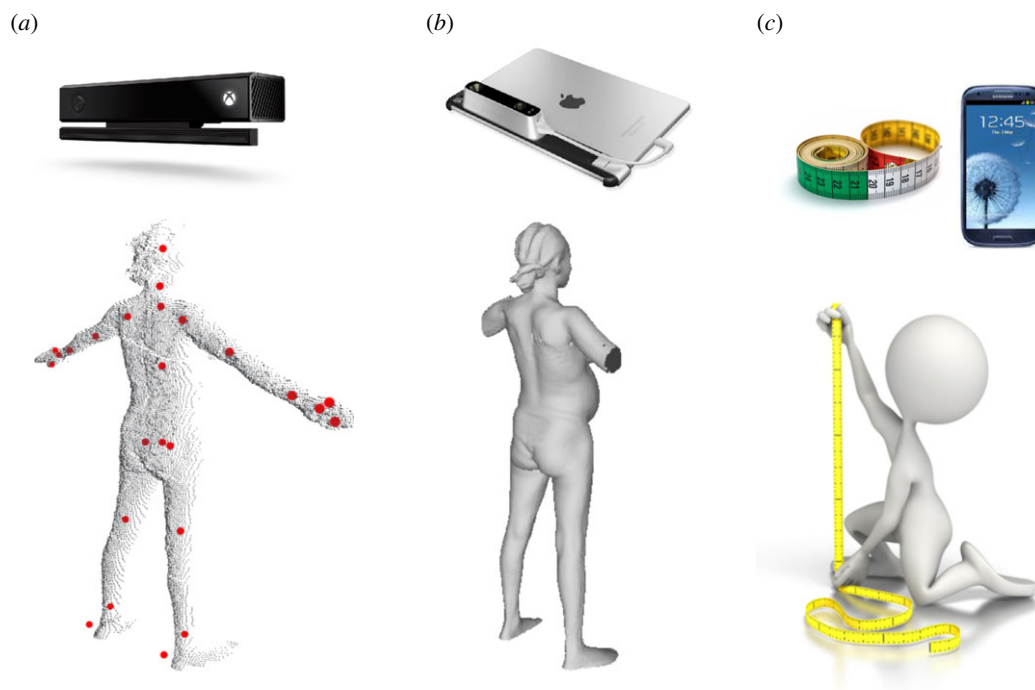


**Figure 1.** Illustrative comparison of the (a) Kinect-, (b) Structure- and (c) tape measure-based tools to assess the risk of CPD. The Kinect camera is operated with a standard laptop and the Structure is operated with an iOS- or Android-based smartphone or tablet. The red dots on the Kinect point cloud indicate joint locations detected by Kinect skeletal mapping algorithms, overlaid on the posterior scan. Traditional anthropometry is conducted with anthropometry tools (e.g. tape measure, stadiometer, etc.). A smartphone application may be used for data entry of the traditional anthropometric measurements and calculation of the CPD risk score. (Online version in colour.)

*diameter, waist circumference, hip circumference* and *foot length* were collected following the published methods [14]. The participant was asked to disrobe (except for tight-fitting undergarments) and stand facing the Kinect camera (Kinect V2 sensor, Microsoft, Inc.), with their arms approximately 45° from the ground and legs spread approximately 50 cm apart. Kinect 3D images were collected from the anterior, posterior, left and right sides, with the Kinect camera remaining stationary while the participant adjusted their position. A Structure 3D camera (Occipital, Inc.) was used to collect a 3D point-cloud image of the subject in the same position; the participant remained stationary, as the nurse moved the Structure camera around the subject to collect the 3D image.

After delivery, the pregnancy outcome was collected both via interview of the participant and review of the participant's hospital card; if necessary, the attending health professional was interviewed regarding the indication for C/S. The nurse recorded the date of birth, the method of delivery (vaginal or C/S), whether C/S was scheduled or performed after trial of labour, the reason the C/S was performed, the infant weight, gender and Apgar scores. Gestational age at delivery was determined and any complications for the mother or the child during labour and delivery were noted. Based on the outcome of the current pregnancy, subjects were categorized into three groups: CPD-related C/S, non-CPD-related C/S or vaginal delivery (VD). We excluded non-CPD-related C/S from analysis; subjects were grouped as CPD (those delivering via a CPD-related C/S) or VD (those having a vaginal delivery).

## 2.2. Three-dimensional image analysis

### 2.2.1. Kinect scan analysis

The Kinect software algorithms (Kinect SDK for Window, 2.0, Microsoft, Inc.) determined the location of 25 key joints from the 3D model, which are tracked in real time in three dimensions to quantify movement. From the skeletal maps, we extracted the following features: *head height, face height, shoulder height, hip*

*height, shoulder width* and *hip width*. From the 3D point cloud surface maps, an automated MATLAB® code was developed to identify key landmarks (figure 2), from which the following anthropometric measurements were determined: *height, shoulder height, waist height, iliac height, symphysis height, hip height, shoulder diameter* (measured as the distance between the left and right arm pit), *waist diameter* (measured as the smallest diameter of the torso), *iliac diameter, hip diameter* (measured as the widest diameter in the pelvic area), five diameters (*Torso Diameter 1, 2, 3, 4* and *5*) equally spaced between the hip and shoulder, *fundal height, fundal volume* and *belly height*. In addition to assessing measurements from individual views, we also calculated several ratios of measurements.

### 2.2.2. Structure scan analysis

The Structure scan produces a 3D model of the participant, from which key landmarks were identified and the following anthropometric measurements were determined, using algorithms similar to those used with the Kinect 3D model: *height, shoulder height, waist height, iliac height, S1 height, hip height, symphysis height, shoulder diameter, waist diameter, iliac diameter, hip diameter*, five diameters (*Torso Diameter 1, 2, 3, 4* and *5*) equally spaced between the hip and shoulder, *waist circumference, hip circumference, external conjugate, fundal height* and *fundal volume*. Several ratios of measurements were also calculated.

## 2.3. Cephalopelvic disproportion risk score development

Following Gleason *et al.* [14], the risk scores were defined as

$$R^j = \beta_0 + \sum_{i=1}^N \beta_i z_i, \quad (2.1)$$

where  $j = T, K, S$  denotes the risk assessment modality (tape measure, Kinect, Structure),  $z_i = (\mu_i - x_i)/\sigma_i$  denotes z-score for the  $i$ th feature (except age, for which the raw values were used),  $\beta_0$  and  $\beta_i$  are model parameters,  $x_i$  are the values of the

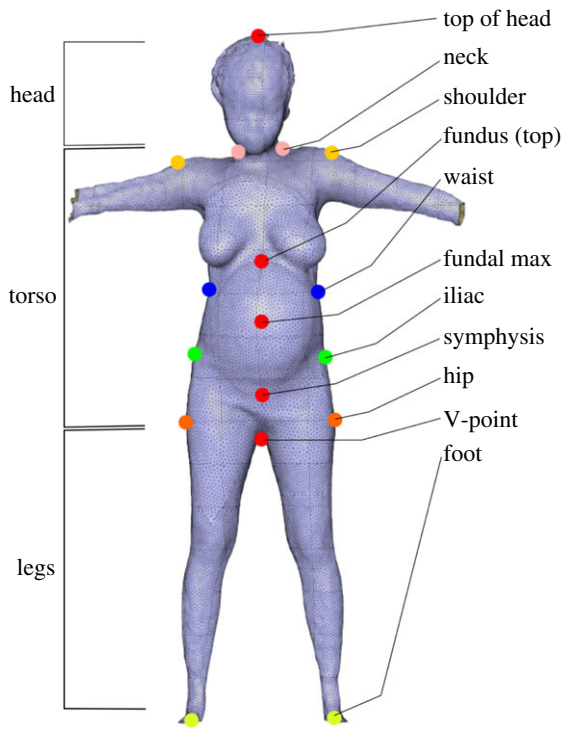


**Figure 2.** Illustration of the key landmarks identified from 3D point cloud image via custom algorithms. These landmarks guide additional custom algorithms to take 3D image-based anthropometric measurements. (Online version in colour.)

features  $f_i$  (e.g.  $f_i = \text{height}$ ,  $x_i = 155$  cm) measured with the respective tool,  $\mu_i$  and  $\sigma_i$  are the mean and standard deviation of the feature values across all subjects. For all data, a Grubb's test for outliers was performed and outlier data points were removed from the dataset. Equation (2.1) represents  $n_p = \ell_j! / (k!(\ell_j - k)!)$  possible permutations of feature sets and parameters that may be calculated for each value of  $k$  for all subjects, where  $\ell_j$  is the total number of features considered for inclusion in the model and  $k$  is the actual number of features included in the model. The best fit parameters ( $\beta_o$  and  $\beta_i$ ) for all  $n_p$  possible permutations of feature sets were determined using the *glmfit* MATLAB<sup>®</sup> subroutine. For each of the  $n_p$  parameter sets, for each value of  $k$ , the *perfcurve* MATLAB<sup>®</sup> subroutine was performed to generate a receiver-operator characteristic (ROC) curve. Note that, for Kinect, because  $n_p$  was too large to evaluate all permutation sets, the feature elimination routine of Gleason *et al.* [14] was employed.

Let us define the following metrics:

$$\begin{aligned} \text{TPR} &= \frac{\text{TP}}{n_{\text{CPD}}}, \text{FNR} = \frac{\text{FN}}{n_{\text{CPD}}}, \text{TNR} = \frac{\text{TN}}{n_{\text{VD}}}, \text{ and} \\ \text{FPR} &= \frac{\text{FP}}{n_{\text{VD}}}, \end{aligned} \quad (2.2)$$

where TPR is the true-positive rate (also known as *sensitivity*), TP is the number of true-positive cases (i.e. CPD cases that score as at risk),  $n_{\text{CPD}}$  is the total number of CPD cases, FNR is the false-negative rate, FN is the number of false-negative cases (i.e. CPD cases that do not score as at risk), FPR is the false-positive rate, FP is the number of false-positive cases (i.e. vaginal deliveries that score as at risk),  $n_{\text{VD}}$  is the total number vaginal deliveries, TNR is the true-negative rate (also known as *specificity*) and TN is the number of true-negative cases (i.e. vaginal deliveries that do not score as at risk). From equation (2.2), it can be seen that  $\text{TPR} = 1 - \text{FNR}$  and  $\text{TNR} = 1 - \text{FPR}$ . The likelihood ratio for CPD is defined as  $\text{LR}_{\text{CPD}} = \text{TPR}/\text{FPR}$ .

We developed two risk models. The first risk model (model 1) identified a single set of features and parameter values that maximized the area under the ROC, denoted AUC. The second risk model employed three models to maximize the detection rate and triage rate of the CPD risk assessment for each modality; each model had a different set of characteristics (denoted generally as  $C$ ). For model 2, we identified the model (denoted model 2.1) that maximized TNR at a false FNR of 0%; i.e.  $C = \text{TPR}@FNR = 0\%$  (figure 3). With model 2.1, we sought to 'triage' as many low-risk subjects as possible, without incorrectly classifying any CPD cases as low risk. Next, we identified model 2.2 that maximized the TPR at an FPR of 5%; i.e. we sought a model that detected as many high-risk subjects, while classifying less than 5% of vaginal deliveries as high risk. On the remaining subjects that were not triaged by model 2.1 or scored as high risk using model 2.2, we applied model 1.

## 2.4. Model training, validation and testing

CPD cases and VD controls were randomized, using the default *randperm* random number generator command in MATLAB<sup>®</sup>; the first 20% of subjects in the randomized sample were assigned as the testing set and the remaining 80% were assigned as the training set. Training and validation were performed on the training set. After the most predictive model was identified, based on the training set, these features and parameters were applied to the testing set to assess the model's predictive capability. For each of the  $n_p$  parameter sets, for each value of  $k$ , the characteristic  $C$  was calculated with the *perfcurve* MATLAB<sup>®</sup> subroutine and the best model was defined as the feature set and model parameters with the greatest  $C$ , denoted  $C_{\text{best}}$ , based on the training dataset. To identify the models expected to have the highest predictive capabilities, we evaluated the optimism,  $O$ , following the approach of Harrell *et al.* [14,15]. Briefly,  $n_B = 1000$  non-parametric bootstrap samples were generated from the original training set. For each bootstrap sample set, the top feature sets were selected and the model parameters ( $\beta_{o,b}$  and  $\beta_{i,b}$ ), for models 1, 2.1 and 2.2, were identified and the value of  $C$  for each bootstrap sample, denoted  $C_{b,\text{boot}}$ , was calculated. The feature sets and fitted model parameters ( $\beta_{o,b}$  and  $\beta_{i,b}$ ) were then applied to the original dataset and the  $C$ , denoted  $C_{b,\text{orig}}$ , was calculated. The optimism was calculated as  $O = (1/n_B) \sum_{b=1}^{n_B} (C_{b,\text{boot}} - C_{b,\text{orig}})$ . The adjusted  $C$ , denoted  $C_{\text{adj}}$ , which represents the expected value of  $C$  if the model was applied to a new dataset (i.e. the predictive capability), was calculated as  $C_{\text{adj}} = C_{\text{best}} - O$ . For each number of features,  $k$ ,  $O$  and  $C_{\text{adj}}$  were calculated for the top 1000 feature sets that yielded the highest  $C_{\text{best}}$ . The most predictive model, based on the training set, was defined as the model with the highest  $C_{\text{adj}}$ . This model was then applied to the testing set to calculate  $C_{\text{test}}$ . In summary, the training step determined the feature sets and parameters with the highest  $C_{\text{best}}$ , the validation step identified the most predictive model as that with the highest  $C_{\text{adj}}$  and the testing set calculated the  $C_{\text{test}}$  using the feature set and model (determined from training set) applied to the testing set.

## 2.5. Assessing predictive capabilities

To assess the predictive capability, we used a four-point risk score contingency table (*very high*, *high*, *moderate* and *mild* risk) based on the risk scores from the final model applied to the complete dataset with the features and parameters. The *very high-high* cut-off was the highest risk value where the FPR was less than or equal to 5%. We define our *detection rate* as the TPR of subjects scored as *very high* risk. The *high-mild* cut-off was defined as the risk score associated with the highest Youden's  $J$ -statistic,  $J = \text{TPR} - \text{FPR}$ , which represents distance between the ROC and a diagonal line from [0,0] to [1,1] on the ROC curve. The *mild-low* cut-off was the highest risk value

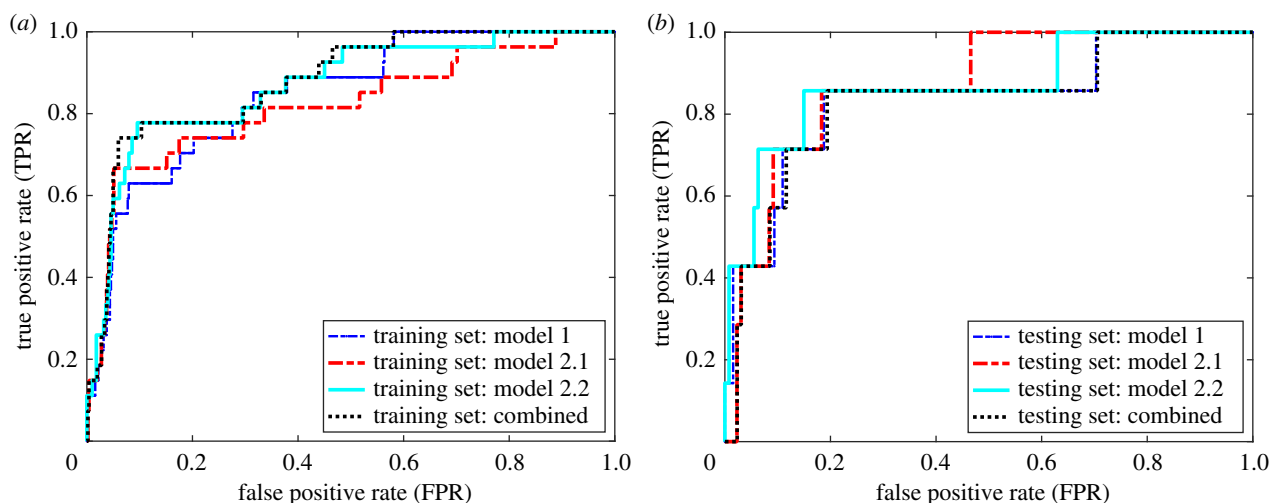


**Figure 3.** Illustration of the three-model approach. Models that optimize the triage rate (model 2.1, red line), the detection rate (model 2.2, cyan line) and the AUC (model 1, blue line) are combined into a single model (model 2, black dotted line), to maximize the triage rate, detection rate and AUC. (a) The training set and (b) the model, fitted with the training set, applied to the testing set. (Online version in colour.)

where  $\text{TPR} = 1$ . We define our *triage rate* as subject that score as low risk.

## 2.6. Statistical analysis

For continuous variables, a two-sample *t*-test was performed ( $p < 0.05$ ). Statistical analysis was performed in MATLAB® (MathWorks).

## 3. Results

### 3.1. Pregnancy outcomes

Of the 810 primigravida recruited for anthropometry and Kinect imaging, 656 of these subjects were also imaged with the Structure 3D camera. Of the 810 women, 34 (4.2%) women delivered via C/S due to CPD, 655 (80.9%) delivered vaginally (VD) and 121 (14.9%) delivered via C/S for reasons other than CPD. Kinect 3D images were collected for 31 CPD cases and 610 vaginal deliveries; the missed subjects arose due to the loss of power in the exam room, technical difficulties in operation or low-quality images. Structure 3D images were collected for 26 CPD cases and 532 vaginal deliveries. The Structure 3D camera was introduced partway through the study, after the first 148 subjects were recruited. A majority of the anthropometric measurements, made with a tape measure and the Kinect and Structure 3D cameras, were significantly different between the CPD and VD groups (tables 1–3; electronic supplementary material, tables S1.csv and S2.csv).

### 3.2. Cephalopelvic disproportion risk assessment

The AUC for tape measure, Kinect and Structure were 0.868, 0.846 and 0.889 for model 1, respectively, and 0.871, 0.908 and 0.918 for model 2, respectively (figures 4 and 5 and table 4). In general, model 2 outperformed model 1 across the indicators (AUC, detection rate and triage rate). The detection rates at 5% FPR for tape measure, Kinect and Structure were 53%, 47% and 48% for model 1, respectively, and 53%, 61% and 64% for model 2, respectively. The triage rates at 0% FNR for tape measure, Kinect and Structure were 24%, 17% and 53% for model 1, respectively, and

30%, 56% and 63% for model 2, respectively. When applied to the testing set, these models showed good consistency with the predictions from the training set; these results were consistent with the optimism predicted using our validation strategy.

The four-point contingency table for model 2 (table 5) shows that 77%, 80% and 84% of CPD cases scored as either *very high* or *high* risk, at FPR of 10%, 15% and 11%, respectively, for tape measure, Kinect and Structure. Note that, after removing outliers, the number of subjects included in the risk calculations reduced slightly; cf. tables 1–3 with 5. Perhaps the most relevant difference between the tape measure tool and the 3D camera tools is in the number of subjects in the low-risk (triage) group, with more subjects being scored with the less definitive, more ambiguous diagnosis of *mild* risk for the tape measure tool. As a result, 57% of the subjects (calculated as  $(8 + 372)/(34 + 632)$  from table 5) were scored as *mild* risk with the tape measure tool, compared to 29 and 25% with the Kinect and Structure tools.

## 4. Discussion

CPD-related obstructed labour poses a major global health burden that contributes significantly to maternal and perinatal mortality and morbidity. Ethiopia has a high incidence of CPD-related obstructed labour, low ANC coverage, low rate of attended deliveries and a large portion of the population without nearby access to emergency C/S. Current strategies to assess CPD risk have limited scale-up potential in the developing world.

Over the last century, much effort has been dedicated to developing methods to accurately assess the risk of CPD, prior to labour, including clinical and radiological pelvimetry and anthropometry. *Clinical pelvimetry* assesses the size of the pelvic cavity by means of the systematic vaginal palpation of specific bony landmarks in the pelvis. This technique requires highly skilled personnel, is subjective and shows low predictive capability [16–18]. Further, given that Ethiopia's densities of doctors (0.025/1000 people) and nurse/midwifery personnel (0.236/1000 people) are among the lowest in the world [19], the number of qualified personnel in Ethiopia is too low to effectively scale this strategy. *Radiological pelvimetry*

**Table 1.** Tape measure-based anthropometry results. Values highlighted in italics indicate statistically significant differences ( $p < 0.05$ ) across groups. The three columns to the left provide the model parameters,  $\beta_0$ , listed directly under the model name, and  $\beta_i$  for the corresponding features listed in the left-most column. The dash symbol (—) indicates that this feature was not included in the corresponding model. BMI, body mass index; circ., circumference.

feature	CPD ( <i>n</i> = 34)	VD ( <i>n</i> = 655)	<i>p</i> -value	model 1 −5.975	model 2.1 −5.800	model 2.2 −3.710
age (years)	25.0 ± 4.0	23.0 ± 3.3	0.001	0.08529	0.08634	—
weight (kg)	65.8 ± 10.9	61.4 ± 8.6	0.005	—	—	—
<i>tape measurements</i>						
height (cm)	154.5 ± 5.0	158.6 ± 5.6	0.000	—	—	1.733
shoulder height (cm)	128.4 ± 5.0	131.5 ± 5.2	0.001	—	—	—
waist height (cm)	91.3 ± 4.7	95.9 ± 4.8	0.000	−0.9011	−0.9250	−0.9682
hip height (cm)	86.0 ± 4.7	88.9 ± 4.7	0.000	—	—	—
head circumference (cm)	56.4 ± 1.6	56.3 ± 2.4	0.69	5.205	0.2628	—
shoulder diameter (cm)	38.5 ± 2.7	38.7 ± 2.5	0.57	—	—	−5.846
waist circumference (cm)	102.7 ± 6.1	97.8 ± 7.1	0.000	−8.508	−6.257	—
hip circumference (cm)	99.2 ± 9.3	96.2 ± 6.5	0.009	—	6.641	2.891
foot length (cm)	23.4 ± 1.2	24.0 ± 1.2	0.003	—	—	—
<i>ratios of measurements</i>						
BMI	27.5 ± 4.3	24.4 ± 3.1	0.000	0.6824	—	0.9406
waist-to-hip ratio	1.05 ± 0.09	1.02 ± 0.05	0.001	6.453	4.960	—
head circ.-to-height ratio	0.37 ± 0.01	0.36 ± 0.02	0.002	−6.008	—	2.254
hip circ.-to-hip height ratio	1.16 ± 0.12	1.08 ± 0.08	0.000	—	—	—
hip circ.-to-height ratio	0.64 ± 0.06	0.61 ± 0.04	0.000	7.722	—	—
shoulder diameter-to-hip circ.	0.39 ± 0.04	0.40 ± 0.03	0.013	−0.4359	—	6.726
head circ.-to-hip circ.	0.58 ± 0.06	0.59 ± 0.04	0.14	—	—	−2.953
(hip-to-shoulder length)-to-hip height	0.49 ± 0.04	0.48 ± 0.06	0.43	—	—	—
head circ.-to-foot length ratio	2.41 ± 0.14	2.35 ± 0.14	0.009	—	—	—

uses X-ray, magnetic resonance imaging (MRI) and computed tomography (CT) to provide accurate quantification of the pelvic passage and fetal size, from which a number of CPD risk scores have been proposed [20–27]. MRI and CT are cost prohibitive in low-resource settings and a majority of mothers in the developing world do not have access to MRI or CT. Further, X-ray radiation exposure to the fetus poses an unwanted health risk and may represent a significant barrier to widespread scale-up in the developing world. In the developed world, assessment of fetal size is routinely done via ultrasound imaging; ultrasound does not provide information on pelvic dimensions. Ultrasound technology and expertise are also limited in most low-resource settings. Further, the accuracy of radiological pelvimetry at predicting CPD-related obstructive labour is controversial and lacks testing via rigorous randomized trials [20,28].

Height has long been recognized as a risk indicator for CPD [29–31] across multiple nationalities and regions of the world [29,32–42], including sub-Saharan Africa [31,43–53]; however, the sensitivity and specificity of height as a predictor of CPD are generally only fair at best [31,34, 38,45,47,51,53–59]. Other anthropometric measurements or combinations of measurements have also been identified as potential risk indicators for CPD, including foot length [32,42,49,52,60], shoulder diameter [42], lower limb length [49], BMI [39,61–64], maternal head circumference-to-height ratio [39] and external pelvimetry (e.g. external intercrestal, interspinous, intertrochanteric and

intertuberous transverse pelvic diameters, anteroposterior external conjugate, and transverse and vertical diagonals of the Michaelis sacral rhomboid area) [35,41,42,52,58]. Published anthropometric-based CPD risk scores only show fair predictability and have not been rigorously employed in clinical practice. Measurements are prone to measurement errors and inter- and intra-user variability [65–68].

Taken together, there is a pressing clinical need to identify novel, low-cost, safe, easy-to-use, scalable methods for timely and accurate assessment of risk of obstructed labour from CPD in low-resource settings. Accurate diagnosis of CPD, well before the onset of labour, using resource-appropriate tools, would allow at-risk mothers to be referred for delivery in a setting where emergency C/S is an option. This paper describes novel innovations designed to address this clinical need.

#### 4.1. Innovation 1: three-dimensional camera-based anthropometry

Our first innovation employs low-cost 3D cameras to generate 3D models of pregnant women, from which anthropometric measurements are automatically extracted via our novel image processing algorithms and used to calculate our novel CPD risk score to identify at-risk mothers. A Kinect V2 sensor, combined with a laptop, was used to generate digital 3D geometric models of pregnant women. Scans that take less than 60 s to collect (30 frames  $s^{-1}$ ) pose no risk for

**Table 2.** Kinect-based anthropometry results. Values highlighted in italics indicate statistically significant differences ( $p < 0.05$ ) across groups. The three columns to the left provide the model parameters,  $\beta_0$  listed directly under the model name and  $\beta_1$  for the corresponding features listed in the left-most column. The dash symbol (—) indicates that this feature was not included in the corresponding model.

feature	CPD ( $n = 31$ )	VD ( $n = 610$ )	$p$ -value	model 1 — 6.979	model 2.1 — 3.679	model 2.2 — 5.654
age	25 ± 4	23 ± 3	0.000	0.1347	—	0.0739
weight (kg)	65.8 ± 10.2	61.4 ± 8.7	0.006	—	0.3158	—
<i>measurements from skeletal mapping</i>						
SM: head height (cm)	146.6 ± 4.9	150.2 ± 6.6	0.003	—	—	—
SM: face height (cm)	133.1 ± 4.8	136.8 ± 6.2	0.001	—	—	— 1.264
SM: shoulder height (cm)	125.8 ± 4.9	129.4 ± 6.1	0.002	—	—	—
SM: hip height (cm)	77.7 ± 5.1	83.0 ± 5.2	0.000	—	— 1.148	—
SM: shoulder width (cm)	28.6 ± 2.5	27.9 ± 2.0	0.07	—	—	2.569
SM: hip width (cm)	12.5 ± 1.3	12.6 ± 1.0	0.79	—	—	—
<i>measurements from 3D point-cloud</i>						
3D: height (cm)	155.6 ± 5.3	159.0 ± 7.3	0.012	—	—	—
3D: shoulder height (cm)	121.4 ± 5.6	125.4 ± 6.0	0.000	—	2.730	—
3D: waist height (cm)	102.0 ± 6.4	106.1 ± 6.2	0.000	—	—	0.4868
3D: iliac height (cm)	82.8 ± 5.4	87.2 ± 5.0	0.000	—	— 0.4469	—
3D: symphysis height (cm)	79.7 ± 5.8	85.3 ± 5.7	0.000	— 0.7362	—	—
3D: hip height (cm)	69.8 ± 6.9	74.0 ± 4.9	0.000	—	0.3995	—
3D: shoulder diameter (cm)	30.5 ± 1.9	30.1 ± 2.3	0.28	—	— 3.810	— 1.604
3D: waist diameter (cm)	24.4 ± 2.5	23.5 ± 2.1	0.016	—	0.5221	— 0.1861
3D: iliac diameter (cm)	33.5 ± 3.0	32.4 ± 2.3	0.011	—	—	—
3D: hip diameter (cm)	36.0 ± 3.0	35.1 ± 2.6	0.08	—	—	—
3D: torso diameter 1 (cm)	33.2 ± 3.0	32.6 ± 3.2	0.27	—	—	—
3D: torso diameter 2 (cm)	35.1 ± 2.4	34.3 ± 2.6	0.09	—	—	— 0.1761
3D: torso diameter 3 (cm)	30.1 ± 3.5	29.7 ± 3.0	0.51	—	—	—
3D: torso diameter 4 (cm)	25.0 ± 2.6	24.1 ± 2.2	0.029	—	— 0.4033	—
3D: torso diameter 5 (cm)	30.1 ± 4.6	28.9 ± 2.8	0.034	—	—	—
3D: belly height (cm)	24.5 ± 5.3	22.4 ± 5.2	0.026	—	—	—
3D: fundal height (cm)	35.8 ± 5.7	32.1 ± 4.6	0.000	—	—	—
3D: fundal volume (cm)	0.4 ± 0.2	0.3 ± 0.1	0.000	0.3503	—	0.4779
<i>ratios of measurements</i>						
hip height-to-hip diameter (3D)	2.0 ± 0.2	2.1 ± 0.2	0.001	—	—	— 0.4378
hip height-to-hip width (SM)	6.2 ± 0.7	6.6 ± 0.7	0.000	— 0.2881	0.2918	—
belly height-to-hip diameter (3D)	0.7 ± 0.1	0.6 ± 0.2	0.036	—	0.09400	—
belly height (3D)-to-hip width (SM)	2.0 ± 0.5	1.8 ± 0.5	0.006	—	—	0.8422
hip height-to-(hip-to-shoulder) (SM)	1.6 ± 0.2	1.7 ± 0.1	0.000	—	—	—
head height-to-(hip-to-shoulder) (SM)	3.0 ± 0.2	3.2 ± 0.2	0.000	— 0.6134	—	— 0.7463
height-to-belly height (3D)	6.5 ± 1.5	7.4 ± 1.6	0.004	0.4485	0.1040	1.121
head height-to-shoulder width (SM)	5.1 ± 0.4	5.4 ± 0.4	0.000	—	—	—
shoulder height-to-shoulder width (SM)	4.4 ± 0.4	4.6 ± 0.3	0.000	—	—	1.970
shoulder height-to-shoulder diameter (3D)	4.0 ± 0.2	4.2 ± 0.3	0.001	—	— 4.568	— 1.786

the mother or fetus, are non-invasive and contact-free and do not require skilled medical personnel to operate or interpret results. The second-generation Kinect V2 sensor, released in 2014 as part of the Xbox One gaming system, includes a high definition (1920 × 1080 pixel) colour camera and a

512 × 424-pixel depth sensor. The depth acquisition is based on the time-of-flight principle where the distance to points on the surface is measured by computing the phase-shift distance of modulated infrared light. Since the depth map is generated with infrared light, it is relatively insensitive

**Table 3.** Structure-based anthropometry results. Values highlighted in italics indicate statistically significant differences ( $p < 0.05$ ) across groups. The three columns to the left provide the model parameters,  $\beta_0$  listed directly under the model name and  $\beta_i$  for the corresponding features listed in the left-most column. The dash symbol (—) indicates that this feature was not included in the corresponding model. WHR, waist-to-hip ratio.

feature	CPD ( <i>n</i> = 26)	VD ( <i>n</i> = 532)	<i>p</i> -value	model 1 −7.4417	model 2.1 −4.237	model 2.3 −6.4754
age	25.0 ± 4.5	22.8 ± 3.3	0.001	0.1334	—	0.09969
weight (kg)	64.9 ± 10.1	60.4 ± 8.1	0.007	—	—	—
<i>anthropometry measures</i>						
height (cm)	154.2 ± 6.0	160.4 ± 6.5	0.000	−2.534	−2.021	—
S1 height (cm)	79.7 ± 5.2	83.6 ± 4.6	0.000	2.247	2.091	—
hip height (cm)	77.0 ± 4.4	80.8 ± 4.3	0.000	—	—	—
symphysis height (cm)	75.0 ± 5.5	81.1 ± 5.5	0.000	−0.9096	−1.058	—
shoulder diameter (cm)	38.7 ± 3.3	37.5 ± 2.6	0.026	—	—	−1.861
waist diameter (cm)	28.5 ± 3.0	27.3 ± 1.9	0.004	—	—	—
iliac diameter (cm)	33.3 ± 3.0	31.8 ± 2.4	0.002	2.520	2.626	0.9101
hip diameter (cm)	35.9 ± 3.2	34.7 ± 2.4	0.020	—	—	—
torso diameter 1 (cm)	35.4 ± 3.2	34.2 ± 3.4	0.08	—	—	0.2823
torso diameter 2 (cm)	36.7 ± 3.3	35.3 ± 2.6	0.010	—	—	0.8183
torso diameter 3 (cm)	33.0 ± 3.3	31.4 ± 2.5	0.001	−1.360	−1.579	—
torso diameter 4 (cm)	29.9 ± 4.3	27.9 ± 2.3	0.000	—	—	0.4089
torso diameter 5 (cm)	36.3 ± 6.0	35.1 ± 5.0	0.25	—	—	−0.8137
hip circumference (cm)	116 ± 13	115 ± 13	0.72	—	—	—
waist circumference (cm)	121 ± 23	114 ± 19	0.07	−0.5341	—	−0.5301
external conjugate (cm)	27.8 ± 3.2	27.0 ± 2.5	0.14	—	0.1232	—
fundal height (cm)	37.5 ± 4.1	34.8 ± 4.9	0.008	—	—	—
fundal volume (cm <sup>3</sup> )	0.430 ± 0.129	0.322 ± 0.120	0.000	—	−2.756	−1.972
<i>ratios of measurements</i>						
WHR	1.02 ± 0.23	1.00 ± 0.19	0.54	0.5478	—	0.5157
hip height-to-hip width	2.17 ± 0.24	2.34 ± 0.18	0.000	—	—	—
height-to-hip width	4.33 ± 0.39	4.64 ± 0.31	0.000	—	—	—
fundal height to hip width	1.05 ± 0.15	1.01 ± 0.15	0.13	—	—	—
fundal volume to hip width	12.5 ± 4.23	9.33 ± 3.51	0.000	0.7511	3.565	2.752
height-to-hip height	2.00 ± 0.06	1.99 ± 0.06	0.18	0.7590	0.5347	—
shoulder height-to-diameter	3.28 ± 0.35	3.56 ± 0.28	0.000	—	−0.5660	−2.093
fundal height-to-external conjugate	1.37 ± 0.23	1.30 ± 0.22	0.12	—	—	—

to changes in ambient illumination, allowing for gaming in dark and well lit rooms. Skeletal mapping algorithms detect 25 Kinect joint locations [69]; while these joint locations are not necessarily accurate locations of the corresponding anatomical joints, they offer repeatable approximations of these locations [70]. One disadvantage of the Kinect sensor platform is that it currently requires external power to operate. Also, the acquisition of a true three-dimensional model of a subject requires the ‘stitching’ together of 3D images from multiple single-view point clouds [14].

The Structure 3D camera uses structured light technology to generate a fully 3D model of objects and is compatible with iOS- and Android-based smartphones. This device has the advantages of improved resolution of 3D surfaces and easier data-acquisition-to-model-generation capability, compared to

the Kinect V2 platform. Further, the smartphone compatibility of the Structure platform does not require a constant power supply, which lends well to scale-up in the developing world. One disadvantage is that the Structure device requires that the participant remain still while being scanned (approx. 60 s); motion during scanning can result in reduced resolution or produce erroneous 3D models. Also, the skeletal mapping capabilities of the Kinect platform are not available for the Structure device. Our results showed that both the Kinect and Structure 3D camera platforms yielded CPD risk scores that outperformed traditional anthropometry; namely, model 2 from the Kinect and Structure showed higher detection rates, triage rates and AUCs, compared to model 2 from the tape measure tool. The Structure 3D platform yielded slightly higher triage rates and AUCs, compared to Kinect,



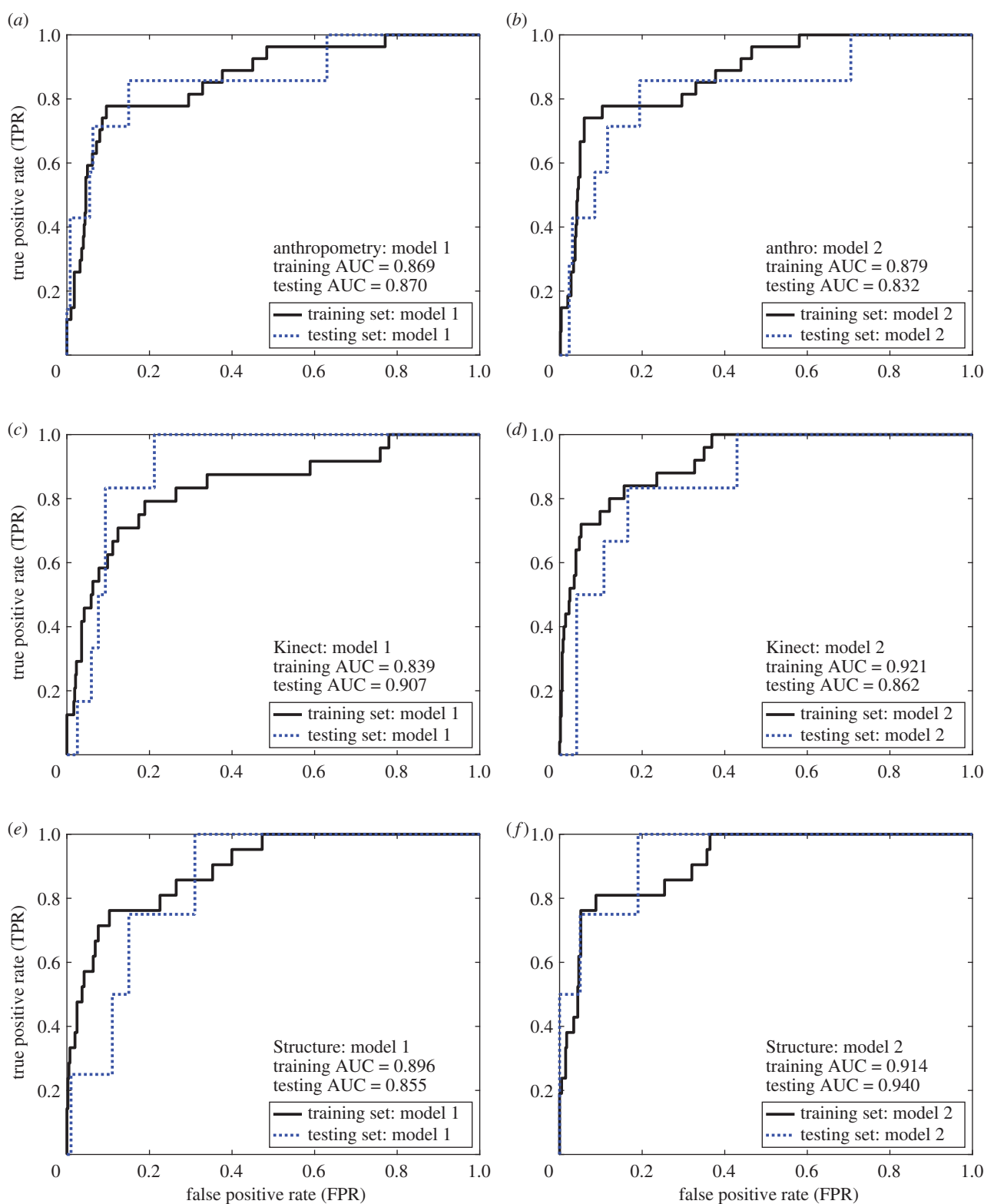


**Figure 4.** ROC curves for models 1 and 2 based on (a,b) tape measure-based, (c,d) Kinect-based and (e,f) Structure-based anthropometry. For each anthropometry method, model 2 outperformed model 1, yielding higher triage rates, detection rates and AUCs; table 4. (Online version in colour.)

perhaps due to the higher resolution camera and easier data-acquisition-to-model-generation.

While the four-point contingency table (table 5) should be interpreted with caution, since 80% of the data in this table was used to train our CPD risk models, this table may be helpful in illustrating how the CPD risk scores may ultimately be used clinically. The Structure 3D platform showed the highest detection and triage rates across modalities, scoring 64% of the CPD cases as very high risk and another 20% of the cases as high risk and 63% of the vaginal deliveries as low risk.

Therefore, with the Structure tool, 43 (8%) of all women (CPD and VD) were scored as very high risk and another 35 (7%) of all women were scored as high risk. Thus, this contingency table suggests that if the 8% of all primigravida that scored as very high risk were referred, 64% of all CPD cases would be captured; if the 15% that scored very high or high were referred, 84% of all CPD cases would be captured, using the Structure tool. Similarly, with the Kinect tool, referring the top 8% (very high risk) would capture 61% of the cases and referring 18% would capture 80% of the cases.

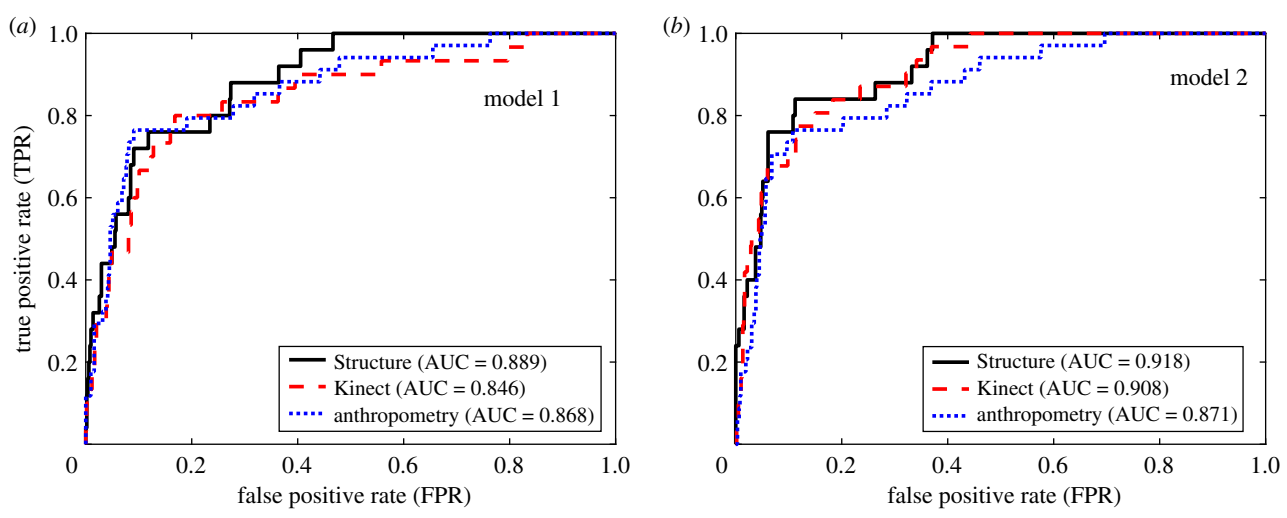


**Figure 5.** (a,b) ROC curves for each anthropometry modality, applied to the entire dataset (i.e. the combined training and testing sets). For both models, the Structure-based anthropometry yielded the highest triage rate, detection rate and AUC. (Online version in colour.)

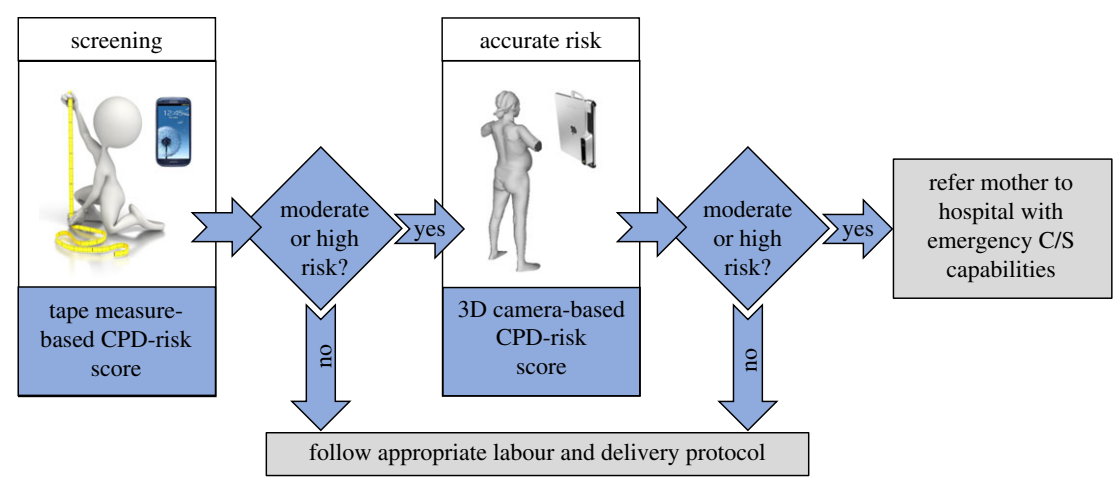


**Figure 6.** Illustration of two-step approach to screening mothers for CPD. Step one: simple screening with a tape measure and smartphone application to calculate tape measure-based risk score. If the tape measure risk score shows low risk, the mother follows best local labour and delivery practice. If the tape measure risk score shows moderate or high risk, the mother receives additional screening via the 3D camera-based tool. Mothers that score as moderate or high risk are referred to a hospital with emergency C/S capabilities; low-risk mothers follow best local labour and delivery practice.

**Table 4.** AUC, detection rate and triage rate for the different anthropometry modalities and different models. ‘Training’, ‘testing’ and ‘combined’ indicate results based on the training, the testing and the entire datasets (training and testing, together), respectively. Note that model parameters were determined by fitting the model parameters to the training dataset. These models, based on fitting of the training dataset, were then applied to testing dataset and the combined dataset.

	AUC			detection rate (very high risk)			triage rate (low risk)		
	training	testing	combined	training (%)	testing (%)	combined (%)	training (%)	testing (%)	combined (%)
<i>anthropometry</i>									
model 1	0.869	0.870	0.868	59	43	53	23	37	24
model 2	0.879	0.832	0.871	67	43	53	42	29	30
<i>Kinect</i>									
model 1	0.839	0.907	0.846	46	17	47	22	79	17
model 2	0.921	0.862	0.908	68	50	61	63	57	56
<i>Structure</i>									
model 1	0.896	0.855	0.889	57	25	48	53	69	53
model 2	0.914	0.940	0.918	62	75	64	64	81	63

**Table 5.** Four-point risk score contingency table. Subjects are scored as very high, high, mild or low risk, based on the calculated risk score.  $LR_{CPD}$ , likelihood ratio for CPD.

four-point risk score contingency table				
	very high	high	mild	low
tape measure risk score				
CPD ( $n = 34$ )	18 (53%)	8 (24%)	8 (24%)	0 (0%)
VD ( $n = 632$ )	34 (5%)	34 (5%)	372 (59%)	192 (30%)
$LR_{CPD} =$	9.84	4.37	0.40	0.00
Kinect risk score				
CPD ( $n = 31$ )	19 (61%)	6 (19%)	6 (19%)	0 (0%)
VD ( $n = 601$ )	32 (5%)	58 (10%)	176 (29%)	335 (56%)
$LR_{CPD} =$	11.51	2.01	0.66	0.00
Structure risk score				
CPD ( $n = 25$ )	16 (64%)	5 (20%)	4 (16%)	0 (0%)
VD ( $n = 508$ )	27 (5%)	30 (6%)	132 (26%)	319 (63%)
$LR_{CPD} =$	12.07	3.39	0.62	0.00

Note that the clinically acceptable FPR and how one might recommend to health systems, clinicians and patients on how to use the diagnostic information will certainly require additional research with regard to cost–benefit analysis, availability of resources and many other factors for a given health system.

The Kinect risk score, in the current paper, has a 61% detection rate at a 5% FPR (i.e. very high-risk group) and an 80% detection rate at a 15% FPR (i.e. high + very high group), which is a significant improvement from our previous work [14]. Our previous paper had a 57% detection rate at a 10% FPR. Therefore, the current work showed a higher detection rate (61 versus 57%) at a lower FPR (5 versus 10%). Further, in our previous paper, the low-risk group was defined at an FNR of 10%, while in the current paper, the low-risk group is defined at an FNR of 0%. The demonstration that a risk score can detect 63% of low-risk subjects, before making a false detection is a significant improvement from the models in our previous publication.

#### 4.2. Innovation 2: combining the tape measure-based tool with a three-dimensional camera-based tool

Our results suggest that our novel anthropometry-based risk score that combines multiple anthropometric measurements shows very good predictability. We demonstrated that the tape measure-based CPD risk score (model 2) was able to accurately detect 53% of the CPD cases as very high risk and another 24% as high risk and accurately triage 30% of low-risk subjects. Our tape measure-based risk score, in the current paper, has a 53% detection rate at a 5% FPR (i.e. very high-risk group) and a 77% detection rate at a 10% FPR (i.e. high + very high group). Our previous paper had a 53% detection rate at a 10% FPR. Therefore, the current work improved the detection rate from 53 to 77% at a 10% FPR.

Given the ultra-low cost and ease of use of the tape measure-based tool, this tool may have tremendous scale-up potential; it simply requires a smartphone application (for entry of measurements and calculation of the risk score) and a tape measure. Although our tape measure-based risk score

is not as accurate as our 3D camera-based risk scores, particularly showing a much lower triage rate, and is likely more prone to measurement errors, this tool may provide an important ultra-low-cost tool for preliminary screening to ‘detect’ and ‘triage’ a significant number of patients and refer remaining subjects for further diagnosis with the more accurate 3D camera-based tool (figure 6). For example, our preliminary data suggest that we may be able to accurately triage 30% of pregnant mothers at low risk and accurately detect 53% of high-risk cases. This leaves approximately two-thirds of the mothers with an ambiguous diagnosis. On the other hand, our data suggest that the Structure 3D camera-based tools can accurately classify 63% of mothers a low risk and accurately detect 60% of the CPD cases. In the latter case, 25% of mothers would be considered as mild risk, compared to 60% of mothers who would score as mild risk with the tape measurement-based tool. We submit that this multi-stage approach could accelerate the access to CPD risk assessment and would require fewer 3D camera-based devices for a given population, while still providing superior risk assessment, compared to the tape measure-based tool alone.

#### 5. Limitations

This study has several limitations. First, while the sample size was fairly large ( $n = 810$ ), given the low prevalence of CPD-related C/S (4.2%), the dataset only includes 34 CPD cases. Learning curves developed based on the current dataset suggest that significant improvements in model predictivity could be achieved with a larger sample size. Second, this dataset is based in one hospital and two health centres in Addis Ababa, Ethiopia. Anthropometric measurements and body features differ across different regions and people groups [71]. Even within the nine regional states of Ethiopia, which represent different ethnic and tribal people groups, we expect to see different correlations between anthropometric measurements and CPD. It is also noteworthy that women in the Tigray region report a nearly three times higher prevalence of obstetric fistula, compared to the rest of Ethiopia, suggesting a heightened CPD risk

in Tegrayan women [2]. Thus, even within Ethiopia, data from different regions are required, not to mention differences that may arise from cultures around the world. Third, all of our data were collected between 36 and 42 weeks of gestation; however, validating CPD risk assessment tools across a wider range of gestational ages will expand the tools' utility. For example, healthcare providers could assess risk at multiple gestational ages, which could help identify risk earlier in pregnancy and provide patients adequate preparation time. Further, given that a majority of women in Ethiopia have three or fewer ANC visits [2], expanding the validated gestational age range would increase the number of pregnant women who access the tool. Fourth, we have not assessed the robustness of the 3D camera-based anthropometry; there is a need to perform inter- and intra-user variability studies to quantify measurement precision.

## 6. Conclusion

This work demonstrates the potential of using 3D camera-based anthropometry and traditional anthropometry to assess the risk of CPD-related obstructed labour in Ethiopia. While these tools show significant potential, broader clinical studies across multiple regions and people groups are required, to

increase the widespread applicability and the predictive capabilities, prior to translation to use in a clinical setting.

**Ethics.** This study was approved by the Institutional Review Board at Addis Ababa University, College of Health Sciences (Protocol no. 054/15/gyn, approved on 3 January 2017).

**Data accessibility.** Traditional anthropometric measurements, Kinect measurements, Structure measurements and pregnancy outcomes are provided as electronic supplementary material files labelled, tables S1.csv and S2.csv.

**Authors' contributions.** All authors contributed to writing and editing the manuscript. L.T., M.Y., S.T. and R.L.G. contributed to data collection activities. L.T., S.A., M.W., N.F., J.B.D. and R.L.G. contributed to data analysis activities.

**Funding.** This work was supported by Grand Challenges Canada (grant no. 0748-03).

**Competing interests.** M.W. and N.F. are employed by LymphaTech, Inc. and J.B.D. owns equity in LymphaTech, Inc. R.L.G., J.B.D. and S.A. were paid consultants to Because of Kennedy to conduct this research. A utility patent (16/143020) is pending for this innovation.

**Acknowledgements.** We gratefully acknowledge the support from Grand Challenges Canada and the Saving Lives at Birth Partners, United States Agency for International Development (USAID), Norwegian Agency for Development Cooperation (Norad), Bill & Melinda Gates Foundation, Grand Challenges Canada, UKaid and the Korea International Cooperation Agency (KOICA).

## References

- WHO. 2015 *Trends in maternal mortality: 1990 to 2015*. Geneva, Switzerland: WHO.
- Ethiopia Demographic and Health Survey 2016. 2016 *Key indicators report*. Addis Ababa, Ethiopia and Rockville, MD: Ethiopian Central Statistical Agency & ICF International.
- El-Hamamy E, Arulkumaran S. 2005 Poor progress of labour. *Curr. Obstet. Gynaecol.* **15**, 1–8. (doi:10.1016/j.curobgyn.2004.09.001)
- WHO. 2005 *The world health report 2005 make every mother and child count*. Geneva, Switzerland: WHO.
- Say L, Chou D, Gemmill A, Tunçalp Ö, Moller AB, Daniels J, Gülmezoglu AM, Temmerman M, Alkema L. 2014 Global causes of maternal death: a WHO systematic analysis. *Lancet Glob. Health* **2**, e323–e333. (doi:10.1016/S2214-109X(14)70227-X)
- Warren C. 2010 Care seeking for maternal health: challenges remain for poor women. *Ethiop. J. Health Dev.* **24**, 100–104. (doi:10.4314/ejhd.v24i1.62950)
- Victora CG *et al.* 2016 Countdown to 2015: a decade of tracking progress for maternal, newborn, and child survival. *Lancet* **387**, 2049–2059. (doi:10.1016/S0140-6736(15)00519-X)
- Tessema GA *et al.* 2017 Trends and causes of maternal mortality in Ethiopia during 1990–2013: findings from the Global Burden of Diseases study 2013. *BMC Public Health* **17**, 160. (doi:10.1186/s12889-017-4071-8)
- Wall LL. 2006 Obstetric vesicovaginal fistula as an international public-health problem. *Lancet* **368**, 1201–1209. (doi:10.1016/S0140-6736(06)69476-2)
- Konje JC, Ladipo OA. 2000 Nutrition and obstructed labor. *Am. J. Clin. Nutr.* **72**, 291S–297S. (doi:10.1093/ajcn/72.1.291S)
- Muleta M. 2004 Socio-demographic profile and obstetric experience of fistula patients managed at the Addis Ababa Fistula Hospital. *Ethiop. Med. J.* **42**, 9–16.
- Dolea C, Abouzahr C. 2003 *Global burden of obstructed labour in the year 2000*. Evidence and Information for Policy (EIP).
- Kelly J. 1995 Ethiopia: an epidemiological study of vesico-vaginal fistula in Addis Ababa. *World Health Stat. Q.* **48**, 15–17.
- Gleason RL *et al.* 2018 A low-cost, easy-to-use platform to assess risk of obstructed labor due to cephalopelvic disproportion in Ethiopia. *PLoS ONE* **13**, e0203865. (doi:10.1371/journal.pone.0203865)
- Harrell FE, Lee KL, Mark DB. 1996 Multivariable prognostic models: issues in developing models, evaluating assumptions and adequacy, and measuring and reducing errors. *Stat. Med.* **15**, 361–387. (doi:10.1002/(SICI)1097-0258(19960229)15:4<361::AID-SIM168>3.0.CO;2-4)
- Anderson DM, Anderson LE, Glanze WD. 2002 *Mosby's medical dictionary*. St Louis, MO: Mosby.
- Adinma JI, Agbai AO, Anolue FC. 1997 Relevance of clinical pelvimetry to obstetric practice in developing countries. *West Afr. J. Med.* **16**, 40–43.
- Maharaj D. 2010 Assessing cephalopelvic disproportion: back to the basics. *Obstet. Gynecol. Surv.* **65**, 387–395. (doi:10.1097/OGX.0b013e3181ecdf0c)
- World Health Organization's Global Health Workforce Statistics. 2017 OECD, supplemented by country data. See <https://data.worldbank.org/indicator/SH.MED.NUMW.P3?view=map&year=2010>.
- Caldwell WE, Moloy HC. 1933 Anatomical variations in the female pelvis and their effect in labor with a suggested classification. *Am. J. Obstet. Gynecol.* **26**, 479–505. (doi:10.1016/S0002-9378(33)90194-5)
- Ball RP. 1936 Roentgen pelvimetry and fetal cephalometry. *Surg. Gynecol. Obstet.* **62**, 798–810.
- Mengert WF. 1948 Estimation of pelvic capacity. *J. Am. Med. Assoc.* **138**, 169–174. (doi:10.1001/jama.1948.02900030001001)
- Abitbol MM, Taylor UB, Castillo I, Rochelson BL. 1991 The cephalopelvic disproportion index. Combined fetal sonography and x-ray pelvimetry for early detection of cephalopelvic disproportion. *J. Reprod. Med.* **36**, 369–373.
- Friedman EA, Taylor MB. 1969 A modified nomographic aid for x-ray cephalopelvimetry. *Am. J. Obstet. Gynecol.* **105**, 1110–1115. (doi:10.1016/0002-9378(69)90134-3)
- Spörri S, Thoeny HC, Raio L, Lachat R, Vock P, Schneider H. 2002 MR imaging pelvimetry: a useful adjunct in the treatment of women at risk for dystocia? *AJR Am. J. Roentgenol.* **179**, 137–144. (doi:10.2214/ajr.179.1.1790137)
- Morgan MA, Thurnau GR, Fishburne JI. 1986 The fetal-pelvic index as an indicator of fetal-pelvic disproportion: a preliminary report. *Am. J. Obstet. Gynecol.* **155**, 608–613. (doi:10.1016/0002-9378(86)90288-7)
- Morgan MA, Thurnau GR. 1992 Efficacy of the fetal-pelvic index in nulliparous women at high risk for fetal-pelvic disproportion. *Am. J. Obstet. Gynecol.* **166**, 810–814. (doi:10.1016/0002-9378(92)91338-B)

28. Rozenberg P. 2007 Is there a role for X-ray pelvimetry in the twenty-first century? *Gynecol. obstét. fertil.* **35**, 6–12. (doi:10.1016/j.gyobfe.2006.09.028)
29. Thomson AM. 1959 Maternal stature and reproductive efficiency. *Eugenics Rev.* **51**, 157–162.
30. Baird D. 1945 The influence of social and economic factors on stillbirths and neonatal deaths. *J. Obst. Gynaecol. British Empire* **52**, 339–366. (doi:10.1111/j.1471-0528.1945.tb07636.x)
31. Everette VJ. 1975 The relationship between maternal height and cephalopelvic disproportion in Dar es Salaam. *East Afr. Med. J.* **52**, 251–256.
32. Kennedy JL, Greenwald E. 1981 Correlation of shoe size and obstetric outcome: an anthropometric study. *Am. J. Obstet. Gynecol.* **140**, 466–467. (doi:10.1016/0002-9378(81)90048-X)
33. Chen HY, Chen YP, Lee LS, Huang SC. 1982 Pelvimetry of Chinese females with special reference to pelvic type and maternal height. *Int. Surg.* **67**, 57–62.
34. Kappel B, Eriksen G, Hansen KB, Hvidman L, Krag-Olsen B, Nielsen J, Videbech P, Wohler M. 1987 Short stature in Scandinavian women—an obstetrical risk factor. *Acta Obstet. Gynecol. Scand.* **66**, 153–158. (doi:10.3109/00016348709083038)
35. Hanzal E, Kainz C, Hoffmann G, Deutinger J. 1993 An analysis of the prediction of cephalopelvic disproportion. *Arch. Gynecol. Obstet.* **253**, 161–166. (doi:10.1007/BF02766641)
36. Hin LY, Khairuddin Y, Ng KB. 1994 The predictive value of extremes of birth weight, mother's height and ethnic origin on the likelihood of emergency caesarean section. *Asia Ocean. J. Obstet. Gynaecol.* **20**, 389–394. (doi:10.1111/j.1447-0756.1994.tb00486.x)
37. McGuinness BJ, Trivedi AN. 1999 Maternal height as a risk factor for caesarean section due to failure to progress in labour. *Aust. N. Zeal. J. Obstet. Gynaecol.* **39**, 152–154. (doi:10.1111/j.1479-828X.1999.tb03360.x)
38. Merchant KM, Villar J, Kestler E. 2001 Maternal height and newborn size relative to risk of intrapartum caesarean delivery and perinatal distress. *Br. J. Obstet. Gynaecol.* **108**, 689–696. (doi:10.1016/s0306-5456(00)00181-9)
39. Connolly G, Naidoo C, Conroy RM, Byrne P, McKenna P. 2003 A new predictor of cephalopelvic disproportion? *J. Obstet. Gynaecol.* **23**, 27–29. (doi:10.1080/0144361021000043173)
40. Khunpradit S, Patumanond J, Tawichasri C. 2005 Risk indicators for caesarean section due to cephalopelvic disproportion in Lamphun hospital. *J. Med. Assoc. Thai.* **88**(Suppl. 2), S63–S68. (doi:10.1111/j.1447-0756.2007.00548.x)
41. Bansal S, Guleria K, Agarwal N. 2011 Evaluation of sacral rhomboid dimensions to predict contracted pelvis: a pilot study of Indian primigravidae. *J. Obstet. Gynaecol. India* **61**, 523–527. (doi:10.1007/s13224-011-0078-8)
42. Benjamin SJ, Daniel AB, Kamath A, Ramkumar V. 2012 Anthropometric measurements as predictors of cephalopelvic disproportion. *Acta Obstet. Gynecol. Scand.* **91**, 122–127. (doi:10.1111/j.1600-0412.2011.01267.x)
43. Kasongo Project Team. 1984 Antenatal screening for fetopelvic dystocias. A cost-effectiveness approach to the choice of simple indicators for use by auxiliary personnel. *J. Trop. Med. Hyg.* **87**, 173–183.
44. Adadevoh SWK, Hobbs C, Elkins TE. 1989 The relation of the true conjugate to maternal height and pbstetric performance in Ghanaians. *Int. J. Gynaecol. Obstet.* **28**, 243–251. (doi:10.1016/0020-7292(89)90725-X)
45. Sokal D, Sawadogo L, Adjibade A. 1991 Short stature and cephalopelvic disproportion in Burkina Faso, West Africa. Operations Research Team. *Int. J. Gynaecol. Obstet.* **35**, 347–350. (doi:10.1016/0020-7292(91)90671-Q)
46. van Roosmalen J, Brand R. 1992 Maternal height and the outcome of labor in rural Tanzania. *Int. J. Gynaecol. Obstet.* **37**, 169–177. (doi:10.1016/0020-7292(92)90377-U)
47. Kwawukume EY, Ghosh TS, Wilson JB. 1993 Maternal height as a predictor of vaginal delivery. *Int. J. Gynaecol. Obstet.* **41**, 27–30. (doi:10.1016/0020-7292(93)90150-U)
48. Tsu VD. 1994 Antenatal screening: its use in assessing obstetric risk factors in Zimbabwe. *J. Epidemiol. Community Health* **48**, 297–305. (doi:10.1136/jech.48.3.297)
49. Van Bogaert LJ. 1999 The relation between height, foot length, pelvic adequacy and mode of delivery. *Eur. J. Obstet. Gynecol. Reprod. Biol.* **82**, 195–199. (doi:10.1016/S0301-2115(98)00232-2)
50. Ould El Joud D, Bouvier-Colle MH, Group M. 2001 Dystocia: a study of its frequency and risk factors in seven cities of West Africa. *Int. J. Gynaecol. Obstet.* **74**, 171–178. (doi:10.1016/S0020-7292(01)00407-6)
51. Brabin L, Verhoeff F, Brabin BJ. 2002 Maternal height, birthweight and cephalo pelvic disproportion in urban Nigeria and rural Malawi. *Acta Obstet. Gynecol. Scand.* **81**, 502–507. (doi:10.1034/j.1600-0412.2002.810605.x)
52. Rozenholc AT, Ako SN, Leke RJ, Boulvain M. 2007 The diagnostic accuracy of external pelvimetry and maternal height to predict dystocia in nulliparous women: a study in Cameroon. *BJOG: Int. J. Obstet. Gynaecol.* **114**, 630–635. (doi:10.1111/j.1471-0528.2007.01294.x)
53. Aitken IW, Walls B. 1986 Maternal height and cephalopelvic disproportion in Sierra-Leone. *Trop. Doct.* **16**, 132–134. (doi:10.1177/004947558601600313)
54. Dujardin B, Van Cutsem R, Lambrechts T. 1996 The value of maternal height as a risk factor of dystocia: a meta-analysis. *Trop. Med. Int. Health* **1**, 510–521. (doi:10.1046/j.1365-3156.1996.d01-83.x)
55. Scott RT, Strickland DM, Hankins GDV, Gilstrap LC. 1989 Maternal height and weight-gain during pregnancy as risk-factors for cesarean-section. *Mil. Med.* **154**, 365–367. (doi:10.1093/milmed/154.7.365)
56. Tsu VD. 1992 Maternal height and age: risk factors for cephalopelvic disproportion in Zimbabwe. *Int. J. Epidemiol.* **21**, 941–946. (doi:10.1093/ije/21.5.941)
57. Burgess HA. 1997 Anthropometric measures as a predictor of cephalopelvic disproportion. *Trop. Doct.* **27**, 135–138. (doi:10.1177/004947559702700305)
58. Liselele HB, Boulvain M, Tshibangu KC, Meuris S. 2000 Maternal height and external pelvimetry to predict cephalopelvic disproportion in nulliparous African women: a cohort study. *BJOG: Int. J. Obstet. Gynaecol.* **107**, 947–952. (doi:10.1111/j.1471-0528.2000.tb10394.x)
59. Sheiner E, Levy A, Katz M, Mazor M. 2005 Short stature—an independent risk factor for Cesarean delivery. *Eur. J. Obstet. Gynecol. Reprod. Biol.* **120**, 175–178. (doi:10.1016/j.ejogrb.2004.09.013)
60. Frame S, Moore J, Peters A, Hall D. 1985 Maternal height and shoe size as predictors of pelvic disproportion: an assessment. *Br. J. Obstet. Gynaecol.* **92**, 1239–1245. (doi:10.1111/j.1471-0528.1985.tb04869.x)
61. Witter FR, Caulfield LE, Stoltzfu RJ. 1995 Influence of maternal anthropometric status and birth-weight on the risk of Cesarean delivery. *Obstet. Gynecol.* **85**, 947–951. (doi:10.1016/0029-7844(95)00082-3)
62. Jensen H, Agger AO, Rasmussen KL. 1999 The influence of prepregnancy body mass index on labor complications. *Acta Obstet. Gynecol. Scand.* **78**, 799–802. (doi:10.1080/j.1600-0412.1999.780911.x)
63. Young TK, Woodmansee B. 2002 Factors that are associated with cesarean delivery in a large private practice: the importance of prepregnancy body mass index and weight gain. *Am. J. Obstet. Gynecol.* **187**, 312–318. (doi:10.1067/mob.2002.126200)
64. Chen G, Uryasev S, Young TK. 2004 On prediction of the cesarean delivery risk in a large private practice. *Am. J. Obstet. Gynecol.* **191**, 616–624. (doi:10.1016/j.ajog.2004.07.004)
65. Ayele B *et al.* 2012 Reliability of measurements performed by community-drawn anthropometrists from rural Ethiopia. *PLoS ONE* **7**, e30345. (doi:10.1371/journal.pone.0030345)
66. Ulijaszek SJ, Kerr DA. 1999 Anthropometric measurement error and the assessment of nutritional status. *Br. J. Nutr.* **82**, 165–177. (doi:10.1017/S0007114599001348)
67. Johnson TS, Engstrom JL, Warda JA, Kabat M, Peters B. 1998 Reliability of length measurements in full-term neonates. *J. Obstet. Gynecol. Neonatal Nurs.: JOGNN/NAACOG* **27**, 270–276. (doi:10.1111/j.1552-6909.1998.tb02649.x)
68. Sicotte M, Ledoux M, Zunzunegui M-V, Ag Aboubacrine S, Nguyen V-K, Group A. 2010 Reliability of anthropometric measures in a longitudinal cohort of patients initiating ART in West Africa. *BMC Med. Res. Methodol.* **10**, 102. (doi:10.1186/1471-2288-10-102)
69. Shotton J *et al.* 2013 Real-time human pose recognition in parts from single depth images. *Commun. ACM* **56**, 116–124. (doi:10.1145/2398356.2398381)
70. Wang Q, Kurillo G, Ofli F, Bajcsy R. 2015 Evaluation of pose tracking accuracy in the first and second generations of Microsoft Kinect. In *2015 Int. Conf. on Healthcare Informatics (ICHI), Dallas, TX, USA, 21–23 October 2015*, pp. 380–389. (doi:10.1109/ICHI.2015.54)
71. Otiemo AO, Mehtre A, Fera O, Lema O, Gebeyehu S. 2016 Developing standard size charts for Ethiopian men between the ages of 18–26 through anthropometric survey. *J. Text. Apparel Technol. Manage.* **10**, 1–10.